Power Differential Protection for Half-Wavelength Transmission Lines - Software in the Loop Analysis

A. F. N. C. Moro, J. A. Santiago, M. C. Tavares

***Abstract*—Half-wavelength transmission line protection is a challenge that hinders the implementation of this technology. However, this line is considered an interesting alternative to transmit bulk power blocks over very long distances and to connect wind and photovoltaic generation to an electrical power system. This study introduces a method to protect a half-wavelength transmission line. The proposed complex plane-based protection algorithm uses a differential complex power in the sequence domain to detect faults along the entire line. The embedded spark-gap mitigation device is properly considered because it is a necessary apparatus to remove severe resonant fault conditions. A time-domain analysis shows that the proposed algorithm achieves robust performance for both internal and external faults.**

***Keywords*—Fault analysis, half-wavelength transmission line, line protection, power differential protection, power system protection, PSCAD.**

I. Introduction

With population growth, there is a growing and continuous demand for energy to provide social and economic development around the world. In this context, the requirement for bulk power transmission over long distances is justified. For distances of approximately 2500 km for systems at 60 Hz or 3000 km at 50 Hz, half-wavelength (HWL) AC transmission lines are feasible [1]. Because the Ferranti effect is negligible, low reactive compensation is required for such a long AC transmission line; therefore, this line is a point-to-point AC link without an intermediate substation. In addition, this technology does not require power electronic-based equipment, such as high voltage direct current (HVDC) transmission lines [2].

The HWL transmission lines have the following primary characteristics [1], [3]: 1) it is appropriate that the line has a length that is marginally longer than half the wavelength to ensure a good stability response; 2) in the central region, the voltage is proportional to the loading level; 3) the current in the central region is nearly the nominal current, regardless of the transmitted power; and 4) the voltages at both terminals are equal and do not vary with the loading level.

Conversely, the HWL line has a peculiar voltage and current response under fault conditions. As the fault location moves towards the central region of the line, the fault current seen by the relays decreases and decreases than the loading current [4]. Faults in the central region have high impedance characteristics [5]. When the fault location moves further towards the remote terminal, high currents are observed by the local relay due to the positive sequence resonant location near 70% to 90% of each line terminal. Faults in those regions can cause severe overvoltages with a fast rate of rise and must be promptly eliminated [6]. Another important aspect is that due to its length, the HWL line has a large distributed capacitance, which is not easy to manage with protection algorithms.

These characteristics prevent proper operation of existing fault detection methods, which cannot be directly applied to the HWL line. Distance protection based on impedance cannot detect faults throughout the line's length [7]. For a large part of the line, faults do not lead to relay tripping, and external faults near the remote terminal are identified as internal faults [7]. Regular current differential protection, which is normally applied to short transmission lines, is inefficient, primarily in the central region of the line that has a high impedance response [8]. In addition, there is a long data communication latency between the terminals [9], as in long HVDC links.

Some studies have tried to develop new protection methods for HWL lines. However, critical problems, including terminal synchronization and communication channel speed, remain [10]. In [11] an adapted differential protection for the HWL line is proposed; however, the authors did not consider overvoltage mitigation when a critical fault occurs, which is strongly suggested in the literature [5], [6], thus preventing a critical analysis of the proposed protection performance.

To contribute to HWL line protection, this document presents a method that is based on power differential protection (PDP) that was developed for regular long transmission lines (400 km) [12], [13]. In this study, the primary goal is to detect faults in the central region of the line, which has a natural high impedance characteristic. Voltage and current phasors are measured at both line ends, and the apparent power variation in the sequence component defines the protection action. In addition, simulations consider the delay between terminal phasor data and a proper representation of the mitigation method based on spark gaps (SG). Previous results were published for the algorithm steady-state performance analysis implemented in the Matlab software [14] proving the validity of the method.

The primary contributions of the paper are as follows:

- Innovative protection algorithm for HWL, modelled and tested in a time domain simulator in software in the loop environment.

This work was supported by the Brazilian institutions CAPES (code 001), CNPq (307237/2020-6; BRICS: 440124-2022/0), and FAPESP 2022/01896-7.

A. F. N. C. Moro is with Federal University of Mato Grosso, Cuiabá, MT, Brazil and University of Campinas, Campinas, SP, Brazil (e-mail of corresponding author: a229997@dac.unicamp.br). J. A. Santiago and M. C. Tavares are with University of Campinas, Campinas, SP, Brazil (e-mail: javsant34@gmail.com; ctavares@unicamp.br).

Paper submitted to the International Conference on Power Systems Transients (IPST2023) in Thessaloniki, Greece, June 12-15, 2023.

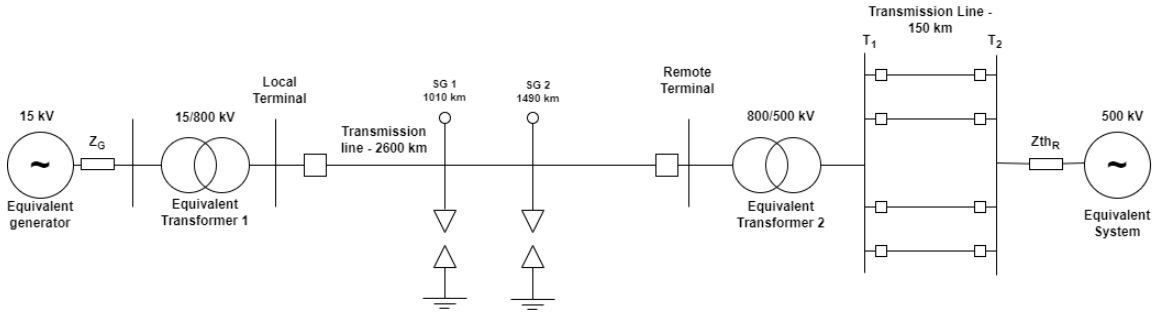

Fig. 1. Test system.

- Analysis of protection speed considering the time delay between the terminals communication channel.
- Fault detection in the middle of the HWL line granted.

II. Main Characteristics of the Simulated System

A. Test System

The test system was simulated in PSCAD and was based on the electrical network presented in [14]. The transmission system was designed to have a surge impedance loading (SIL) of 4800 MVA at an 800 kV 2600 km long line (i.e., a HWL transmission line for a 60-Hz system). The HWL remote terminal is connected to the power system through four 150 km parallel 500 kV transmission lines. All lines were represented with a phase domain frequency-dependent model. The test system is a generation-grid configuration and is shown in Fig.1.

TABLE I
Transmission Lines Parameters at 60 Hz

Electrical Parameters			
	Zero sequence		
	R0	X0	B0
	(Ω/km)	(Ω/km)	(μS/km)
2600 km line	0.3868	1.3478	4.09
150 km line	0.4086	1.3828	3.5171
	Positive/Negative Sequences		
	R1	X1	B1
	(Ω/km)	(Ω/km)	(μS/km)
2600 km line	0.0068	0.1714	9.65
150 km line	0.0161	0.2732	6.038
Electromagnetic Parameters			
		Positive Sequence	Zero Sequence
	γ (km^{-1})	0.0000255 + j 0.001286	0.000333+ j 0.00236
2600 km line	$\mid Zc \mid$ (Ω)	133.3	585.5
	Pc (MW)	4800	-
		Positive Sequence	Zero Sequence
	γ (km^{-1})	0.0000378+ j 0.00128	0.000322 + j 0.00223
150 km line	$\mid Zc \mid$ (Ω)	212.8	640.3
	Pc (MW)	1174	-

Table I shows the electrical parameters of the transmission lines, where γ is the propagation constant, Zc is the characteristic impedance and Pc is the natural power (SIL) of the transmission line. The adopted soil resistivity is 2000 Ω.m. The HWL line was transposed in 9 cycles of 288 km. The power system data are shown in Table II.

SG, a typical surge protection device, is used to take the electric system out of resonance conditions during fault events [5]. Two SGs were installed at 1010 km (SG_1) and 1490 km (SG_2). The values of the SG breakdown voltage are 2.90 pu for SG_1 and 2.92 pu for SG_2, which were set considering the maximum value reached by a three-phase external fault near a remote terminal.

B. HWL fault impedance analysis

The primary characteristic of the HWL transmission line is the point-to-point connection without intermediate substations. In addition, the HWL line has its characteristic fault impedance response produced by its large length. Due to peculiar voltage and current behavior during fault occurrence, conventional protection principles do not apply to HWL lines in a straightforward manner. According to [5], this result can be explained by analysing three important zones in the HWL transmission line. The first (1^{st}) zone, [0 km:1000 km], has an inductive reactance and resistance that is nearly linear; the second (2^{nd}) zone, [1000 km:1500 km], has nonlinear reactance with a zero-crossing and high resistance; the third (3^{rd}) zone, [1500 km:2600 km], has capacitive reactance and resistance that is nearly linear. Also, a resonant condition is observed at approximately 2160 km.

TABLE II
Power System Parameters

Source equivalent impedances				
Source	Zero Sequence (Ω)			
Generation - 15 kV	0.000342 + j 0.011775			
Strong System - 500 kV	7.1187 + j 35.5934			
Source	Positive Sequence (Ω)			
Generation - 15 kV	0.000342 + j 0.011775			
Strong System - 500 kV	1.1864 + j 7.1187			
Equivalent transformer				
Transformer	XR (%)	kV	MVA	Connection
1	11.84	15/800	5500	Δ/Yn
2	10	800/500	5200	Yn/Yn

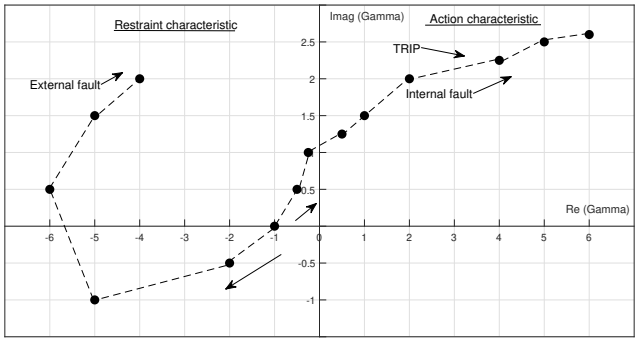

Fig. 2. Complex plane for incremental power ratio.

Therefore, faults in the 1^{st} zone have similar characteristics as faults in conventional-length lines, indicating that conventional distance protection would have an adequate response. However, there are some peculiarities in the 2^{nd} and 3^{rd} zones. Faults in 2^{nd} zone cause small variations in voltage and current, as in high impedance faults in conventional-length lines. There is a critical region in the 3^{rd} zone, which corresponds to a low series impedance during fault. This situation provokes a severe overvoltage when three-phase, phase-to-phase, or phase-to-phase-to-ground faults occur approximately at 85% of the line length from each terminal. Voltage and power will increase quickly with a high rate of rise, jeopardizing the line insulation and the system stability before the protection system can trip the line [5]. In this study, SGs were installed at 1010 km and 1490 km from local terminal as a mitigation method to prevent these resonant faults.

III. Proposed Protection Method

The former algorithm was developed focusing on conventional AC long lines [15], and it is now adapted with respect to the HWL line characteristics. In [14] the method was studied in a phasor domain environment representing a pseudo-dynamic response with Matlab. In this study, the method uses the measured voltage and current phasors at each HWL line terminal to calculate the apparent power in PSCAD simulations. The measured data in both terminals are synchronized. Then, the incremental apparent power at each terminal is obtained to calculate the ratio between them. The algorithm will identify the internal fault according to the ratios in a complex plane. The left half-plane is a restraint characteristic, and the right half-plane is an operation characteristic, with the steady-state point at (-1, 0), corresponding to the pre-fault condition, as shown in Fig. 2. The primary characteristics of the proposed method are described in the following subsections.

A. Phasor Estimation

After acquiring voltage and current data at both terminals, the next step is to estimate the phasors. Before the estimation process, the instantaneous values are filtered by a low pass second-order Butterworth filter with a cut-off frequency of 480 Hz, and sampled in 960 Hz. The calculated phasors are considered perfectly synchronized.

The phasor estimation is made with a cosine filter, which has its coefficients sampled from a cycle of cosine form with an effective response for exponentially decaying DC offset [16]. Considering an instantaneous value, $x(t)$, the fundamental frequency phasor associated is given by (1).

$$\hat{X}_{re}(k) = \frac{\sqrt{2}}{N} \sum_{n=0}^{N-1} x_n \cdot cos(\frac{2\pi n}{N}) \tag{1}$$

where:

N is the number of samples per cycle, $N = 16$;

k is the current phasor index;

n is the current sample;

$\hat{X}_{re}$ is the real part of calculated phasor.

Because the imaginary part is a sine form of cosine filter, the $\hat{X}_{re}$ calculated at the previous N/4 samples is equal to $\hat{X}_{im}$ in the current sample. To calculate the magnitude and the angle of the phasor, (2) and (3), respectively, must be applied.

$$\bar{X} = \sqrt{\hat{X}_{re}^2 + \hat{X}_{im}^2} \tag{2}$$

$$\phi = tg^{-1}(\frac{\hat{X}_{im}}{\hat{X}_{re}}) \tag{3}$$

This nonrecursive method updates consecutive phasors lagging by an angle θ, as in (4)[17].

$$\theta = \frac{2\pi}{N} \tag{4}$$

The rotated phase angles hinder this algorithm because it operates based on phase angles. Therefore, (5) can be used to correct the angles [17].

$$\begin{bmatrix} \hat{X}_{nre}(k) \\ \hat{X}_{nim}(k) \end{bmatrix} = \begin{bmatrix} \cos(k\theta) & \sin(k\theta) \\ -\sin(k\theta) & \cos(k\theta) \end{bmatrix} \cdot \begin{bmatrix} \hat{X}_{re}(k) \\ \hat{X}_{im}(k) \end{bmatrix} \tag{5}$$

where $\hat{X}_{nre}$ and $\hat{X}_{nim}$ are the phasors with the angle correction.

B. Capacitive Current

The naturally distributed capacitance of the transmission line is a problem for HWL line protection and cannot be disregarded, as in short lines. The technique applied uses the transmission line equations with the measured current [18] and voltage [15] at both ends of the line referred to three points, as established by (6) and (7), and shown in Fig.3.

$$\begin{bmatrix} \hat{V}_{TX_p}(k) \\ \hat{I}_{TX_p}(k) \end{bmatrix} = \begin{bmatrix} A & B \\ C & D \end{bmatrix} \cdot \begin{bmatrix} \hat{V}_T(k) \\ \hat{I}_T(k) \end{bmatrix} \tag{6}$$

$$\begin{bmatrix} A & B \\ C & D \end{bmatrix} = \begin{bmatrix} \cosh(\bar{\gamma} \cdot l_{TX_p}) & -\bar{Z}_C \sinh(\bar{\gamma} \cdot l_{TX_p}) \\ -\frac{\sinh(\bar{\gamma} \cdot l_{TX_p})}{\bar{Z}_C} & cosh(\bar{\gamma} \cdot l_{TX_p}) \end{bmatrix} \tag{7}$$

where:

T: the local terminal (L) or remote terminal (R);

X_p: the considered point; and

l_{TX_p}: distance from reference X_p to terminal T [km].

The line terminal voltage and current phasors measured in phase-domain are used to calculate the voltage and current

phasors considering the distances from the terminals to the considered points in the HWL line (X_1 = 1300 km, X_2 = 650 km and X_3 = 1950 km). This technique is applied to reduce the distance between the fault point and the terminals, as explained in [18], and not to calculate the amount of distributed capacitive current. Due to the HWL line characteristic, if we use only one point, the detection near the terminals would be compromised, primarily for the positive sequence [14]. Thus, in this study, we performed the required calculations for the three mentioned points.

C. Sequence Domain Conversion

After the capacitive current calculation, the voltage and current phasors in the phase domain for each X point are converted to the sequence domain using (8). The results for X_2 and X_3 will be used only for positive sequence calculations. Thus, there will be positive sequence phasors for voltage and current at X_1, X_2, and X_3. For zero and negative sequence phasors, there will be phasors only for X_1. This last step is necessary to circumvent the three-phase fault detection near the terminals [14], where there is no use of the zero and negative sequence components.

$$\begin{bmatrix}\hat{V}_{1TX}(k)\\ \hat{V}_{2TX}(k)\\ \hat{V}_{0TX}(k)\end{bmatrix} = \frac{1}{3}\cdot\begin{bmatrix}1 & \bar{a} & \bar{a}^2\\ 1 & \bar{a}^2 & \bar{a}\\ 1 & 1 & 1\end{bmatrix}\cdot\begin{bmatrix}\hat{V}_{ATX}(k)\\ \hat{V}_{BTX}(k)\\ \hat{V}_{CTX}(k)\end{bmatrix} \tag{8}$$

where $\bar{a} = e^{j\frac{2\pi}{3}}$

D. Positive Sequence Voltage Memory

Positive sequence voltage memory is an essential tool to ensure reliability to the protection system, mostly in the case of faults that result in voltages near zero [19]. The factor α is adjusted to control the positive sequence voltage memory that is calculated by (9) and (10).

$$\hat{V}_{1m_X}(k) = \alpha\hat{V}_{1_X}(k) + (1-\alpha)\hat{V}_{1m_X}(k-1) \tag{9}$$

$$\alpha = \frac{1}{MN+1} \tag{10}$$

where:

$\hat{V}_{1m_X}(k)$: Memorized positive sequence voltage for a considered X point;

$\hat{V}_{1_X}(k)$: Positive sequence voltage phasor calculated in the present window for a considered X point;

$\hat{V}_{1m_X}(k-1)$: Positive sequence voltage calculated in the previous window for a considered X point; and

M: The decaying constant in the number of the fundamental cycles.

M is important because this is the variable that will represent the short or long positive sequence voltage memory. In other words, M will determine the portion of $\hat{V}_1(k)$ and $\hat{V}_{1m}(k-1)$ that will result in $\hat{V}_{1m}(k)$. Therefore, M equals 0.1 during the HWL line energization, and after that M goes to 10.

E. Disturbance Detection

Disturbance detection is a necessary action to lock and capture the complex power in a value that was calculated during the steady-state condition (i.e., before the event happened). This stage detects events such as internal and external faults, remote line tripping, large load variation, and others. The disturbance detection will be based on differential instantaneous power, as in (11) and (12). The basic assumption is that during normal operation the instantaneous power does not vary much, meaning that if the power signal is delayed by one cycle (N samples), the mismatch will be small.

$$p(k) = v_a(k)\cdot i_a(k) + v_b(k)\cdot i_b(k) + v_c(k)\cdot i_c(k) \tag{11}$$

$$\Delta p(k) = |p(k) - p(k-N)| \tag{12}$$

where:

$v_f(k)$ and $i_f(k)$ are the instantaneous voltage and current data, respectively, for phases f=[a, b, c];

$p(k)$ is the instantaneous power; and

$\Delta p(k)$ is the differential instantaneous power.

If $\Delta p(k)$ is higher than $0.1\cdot p(k-N)$, then the disturbance is detected and $k = k_L$ denotes the moment when the disturbance is detected.

F. Incremental Complex Power in Sequence Domain

When a fault occurs, an important incremental power is observed at the terminals. First, the complex power in the sequence domain ($\bar{S}_{sTX}(k)$) is calculated by (13), where the subscript s denotes the sequence component.

$$\bar{S}_{sTX}(k) = \hat{V}_{sTX}(k)\cdot\hat{I}_{sTX}(k)^* \tag{13}$$

The $\bar{S}_{sTX}(k)$ are the variables communicated between line terminals. There will be a communication channel latency (δt) that cannot be neglected in simulations. As the HWL transmission line is much longer than conventional transmission lines, algorithms based on two-terminals measures have to address this delay. Fig. 4 shows the communicated variables between the terminals.

The incremental power is calculated in two different ways: when the protection system does not detect any event or when there is disturbance detection.

1) Normal Operation Condition: The incremental complex power for each sequence is calculated by comparing the current calculated complex power with the calculated complex power delayed by one cycle, as presented by (14). For the received variables, the calculation follows (15), where the channel delay (δt [s]) was considered.

$$\Delta\bar{S}_{sLX}(k) = \bar{S}_{sLX}(k) - \bar{S}_{sLX}(k-N) \tag{14}$$

$$\Delta\bar{S}_{sRX}(k-\delta t) = \bar{S}_{sRX}(k-\delta t\cdot Nf) - \bar{S}_{sRX}(k-\delta t\cdot Nf-N) \tag{15}$$

Where f is the system frequency. In (15), the calculation ($\delta t\cdot Nf$) is used to express the delay in a number of samples.

Equations (14) and (15) present the calculation for the local terminal and the variables received in this terminal. The same is calculated for the remote terminal perspective.

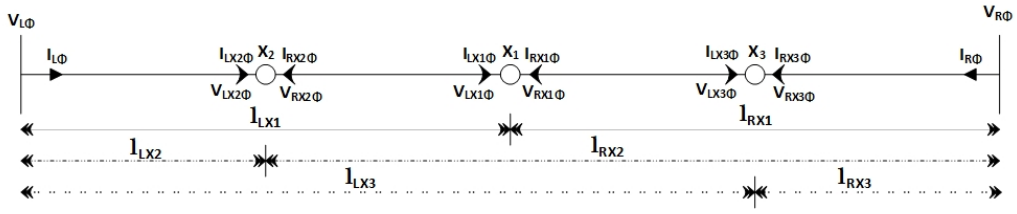

Fig. 3. Currents and voltages measured at the terminals are referred to points X_1, X_2 and X_3.

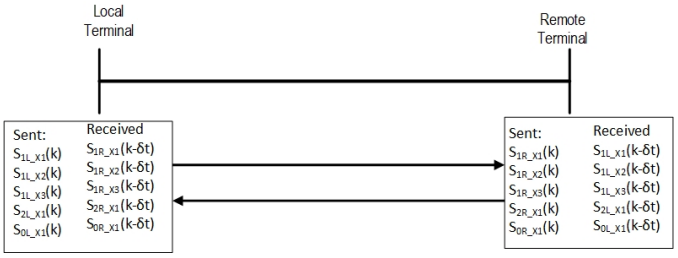

Fig. 4. Communicated variables between line terminals.

2) Disturbance Event: The complex power calculated in the previous cycle is locked in the current window calculation (k_L sample) when an event is identified, as presented by (16).

$$\Delta\bar{S}_{sT}(k) = \bar{S}_{sTX}(k) - \bar{S}_{sTX}(k_L - N) \tag{16}$$

To calculate the ratio between the incremental complex power at each terminal ($\bar{\Gamma}$), the calculated $\Delta\bar{S}_{sT}(k)$ must be higher than an established constraint (Lim_{sT}).

When a disturbance is detected, the limits are locked in the values measured at the time of detection. If an event is identified as an external fault, the established constraints are enlarged to avoid incorrect operations.

If one of incremental complex powers calculated is not greater than Lim_{sT} then the Γ_{sT} is not calculated, and $\bar{\Gamma}_{sT}(k)$ is set to $0 + 1\,j$. If not, $\Gamma_{sT}(k)$ is given by (17) and (18).

$$\bar{\Gamma}_{sL}(k) = \frac{\Delta\bar{S}_{sL}(k)}{\Delta\bar{S}_{sR}(k - \delta t \cdot Nf)} \tag{17}$$

$$\bar{\Gamma}_{sR}(k) = \frac{\Delta\bar{S}_{sR}(k)}{\Delta\bar{S}_{sL}(k - \delta t \cdot N \cdot f)} \tag{18}$$

The complex ratios $\bar{\Gamma}_{sL}$ and $\bar{\Gamma}_{sR}$ are interpreted accordingly in a complex plane, as seen in Fig. 2. If one of the calculated complex ratios is located on the right side of the complex plane and remains there for $N/2$ consecutive samples (8 samples), the fault binary goes up. However, if all $\bar{\Gamma}_{sL}$ and $\bar{\Gamma}_{sR}$ are located on the left side of the plane, no internal fault is issued.

IV. Simulation Results

The method developed in this study was simulated in PSCAD in software in the loop environment. Some scenarios were proposed to test the sensibility, speed, and reliability of the algorithm.

A delay (δt) of 30 ms between the terminals is assumed to consider the data communication delay and the synchronization error in real systems. The propagation speed of the optical fiber channel was considered as 150 km/ms and an additional delay in communication devices to enlarge the signal of 10 ms was added, summing up the delay value used in this study. As the HWL transmission line is too long, this delay cannot be neglected. Similar values are also measured in actual very long HVDC links.

Constraints are given in the pu base of the SIL, and there is an adjustment for each loading level scenario. When an external fault is detected, the algorithm sends a signal to mark the fault condition, and the constraints change to avoid incorrect operations. In addition, for an external fault, there is a change in positive sequence memory, where M is set to 0.1 to reduce the memory. The data are described in Table III.

TABLE III
Differential Power Constraints - PU values

Internal faults				
	Loading level 1.0 SIL		Loading level 0.8 SIL	
	Terminals		Terminals	
Sequences	Local	Remote	Local	Remote
Positive	0.75	0.95	0.75	1.05
Negative	0.16	0.35	0.16	0.40
Zero	0.04	0.08	0.04	0.09
External faults				
Sequences	Local / remote terminals			
Positive	3.0			
Negative/Zero	2.0			

To demonstrate the robustness of the algorithm, internal and external faults are simulated. The faults are applied in half a cycle from 0.7525 s to 0.76 s at each 0.5 ms, totaling 16 cases. For internal fault cases, all fault types are placed at seven different points of the HWL line with fault resistance (R_f) variations and two different loading levels, totalling 3584 simulated cases. Similarly, for external faults, the same fault types will be placed at three different points of a 150 km line, totalling 1536 cases. All cases are summarized in Table IV. The complex plane will be presented for some simulated cases.

Afterward, a statistical analysis provides a comprehensive perspective of the protection speed and reliability.

A. Internal Faults

From each simulated case, the algorithm constantly calculates the ratio between the incremental power of both terminals, obtaining the variables Γ_{sL} and Γ_{sR} for each sequence. To detect internal faults, one of Γ_{sL} or Γ_{sR} must be on the right semiplane of the complex plane.

TABLE IV
SIMULATION PARAMETERS

	Fault location (km)	Fault time (s)	Fault type	Fault resistance (Ω)	Load level (pu)	Total
Internal Fault	144	0.7525 : 0.0005 : 0.76	ABCG; AG; BCG; AC	0.01; 10; 50; 100	0.8; 1	512
	433	0.7525 : 0.0005 : 0.76	ABCG; AG; BCG; AC	0.01; 10; 50; 100	0.8; 1	512
	866	0.7525 : 0.0005 : 0.76	ABCG; AG; BCG; AC	0.01; 10; 50; 100	0.8; 1	512
	1300	0.7525 : 0.0005 : 0.76	ABCG; AG; BCG; AC	0.01; 10; 50; 100	0.8; 1	512
	1444	0.7525 : 0.0005 : 0.76	ABCG; AG; BCG; AC	0.01; 10; 50; 100	0.8; 1	512
	2022	0.7525 : 0.0005 : 0.76	ABCG; AG; BCG; AC	0.01; 10; 50; 100	0.8; 1	512
	2600	0.7525 : 0.0005 : 0.76	ABCG; AG; BCG; AC	0.01; 10; 50; 100	0.8; 1	512
External Fault	0	0.7525 : 0.0005 : 0.76	ABCG; AG; BCG; AC	0.01; 10; 50; 100	0.8; 1	512
	75	0.7525 : 0.0005 : 0.76	ABCG; AG; BCG; AC	0.01; 10; 50; 100	0.8; 1	512
	150	0.7525 : 0.0005 : 0.76	ABCG; AG; BCG; AC	0.01; 10; 50; 100	0.8; 1	512
Total						5120

In all complex plane figures, Γ_{sL} or Γ_{sR} samples that resulted in a protection action will be plotted. Therefore, the figures present a time tag in some numbered samples, where the samples number are the circled number. The purpose of these figures is to show the path that Γ_{sL} or Γ_{sR} made and the time detection.

Fig. 5 and Fig. 6 show an ABCG fault applied in the middle of the HWL line (fault at 0.7525 s; loading level: 1 pu; fault resistance: 0.01 Ω), and only positive sequence is shown. Fig. 5 shows the algorithm response for X_2 calculated from the local terminal. The phase voltages on the local terminal are plotted, and it is possible to verify that the terminal voltage does not decrease, as commonly occurs in conventional long lines during a fault event. Then, the fault signal (FLT) at 0.7525 s goes up, indicating the moment that the fault begins.Γ_{1L} (S_+) detects the first sample in the right semi plane at 0.769 s. After 8 samples (25.5 ms), the trip binary goes up, and after 50 ms the circuit-breaker (BRKL) opens the local terminal of the line. A trip binary is sent to the remote terminal and 30 ms after BRKL was open, the circuit-breaker associated with the remote terminal (BRKR) opens. Thus, the fault is actually removed 105.5 ms after the fault event.

Fig. 6 shows the path of the positive sequence referred to the point X_2. The method will distinguish an internal fault from an external fault by detecting 8 or more consecutive samples in the right semi plane.

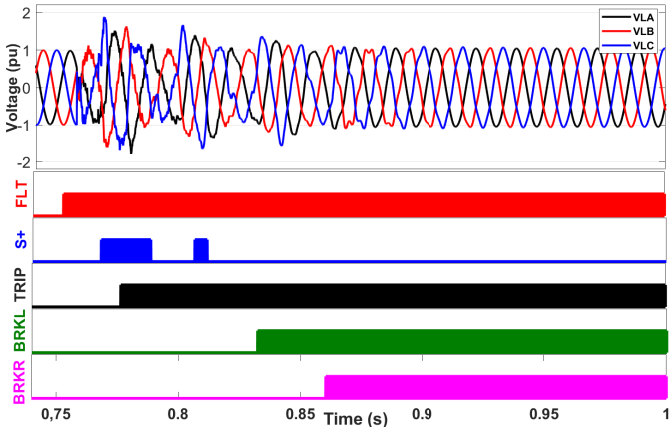

Fig. 5. Phase voltages and protection signals measured at the local terminal (line side) for an ABCG fault at 1300 km - Loading level: 1 SIL; fault resistance: 0.01 Ω.

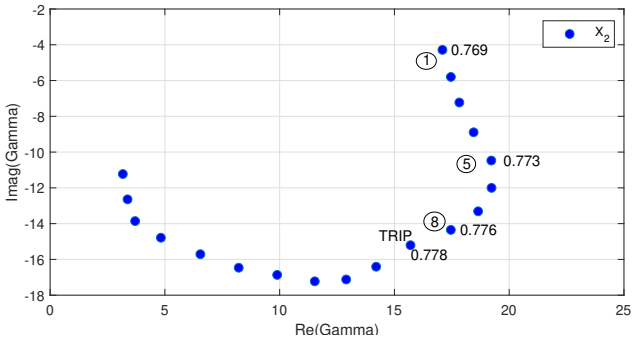

Fig. 6. Complex plane for Γ_{1L} referred to $X2$ for an ABCG fault at 1300 km.

B. External Faults

When an external fault occurs, $\Delta\bar{S}_{sT}$ is lower than the established threshold, meaning that both Γ_{sL} and Γ_{sR} are located at the left semi plane of the complex plane. To demonstrate this case, a 0.01 Ω ABCG fault in terminal T_1 (0 km) of a 150-km-long line was applied. Observing the phase voltages measured at the remote terminal in Fig.7, there is a voltage reduction during fault insertion. The line protection in the faulted line detected the fault, and the associated circuit-breaker opened. The HWL line protection must not operate during external faults or by external circuit-breaker openings. In this case, Γ_{1R} referred to X_3 (signal S_+) entered the right semi plane but was not sufficiently long to cause a protection trip, as shown in Fig.8, whereupon only 7 consecutive samples were in the right semi plane. Therefore, the HWL transmission line circuit-breakers did not operate. For all external fault cases the algorithm did not send a false trip signal.

C. Statistical Analysis

A general statistical analysis was implemented for 1.0 SIL loading condition. Results for the nominal operation are shown in Fig. 9 and Fig. 10, where the average time detection (right side of the graphic) and the success rate (left side of the graphic) are monitored. All types of faults are analysed for each R_f value. Similar results were obtained for 0.8 SIL operating condition.

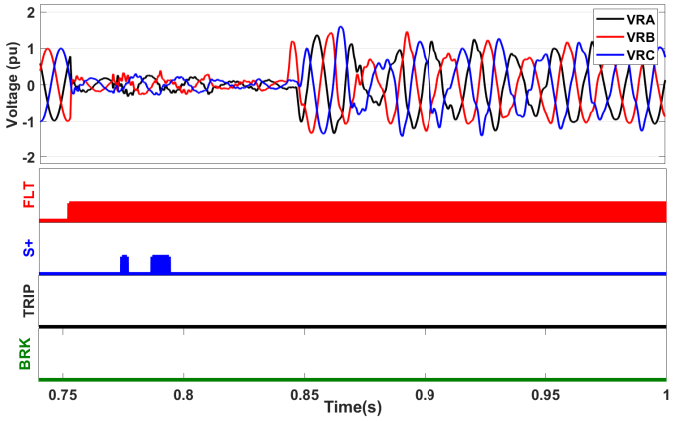

Fig. 7. Phase voltages and protection signals measured at the remote terminal for an ABCG fault on the 150 km line at location 0 km - Fault resistance: 0.01 Ω.

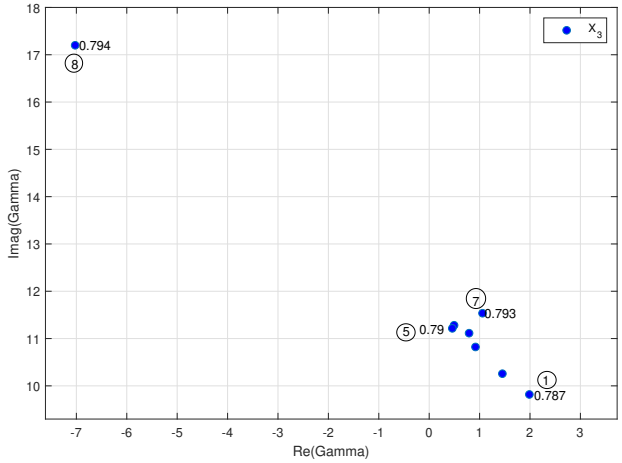

Fig. 8. Complex plane for Γ_{1L} referred to $X3$ for an ABCG fault at terminal T_1 (0 km) of a 150 km line.

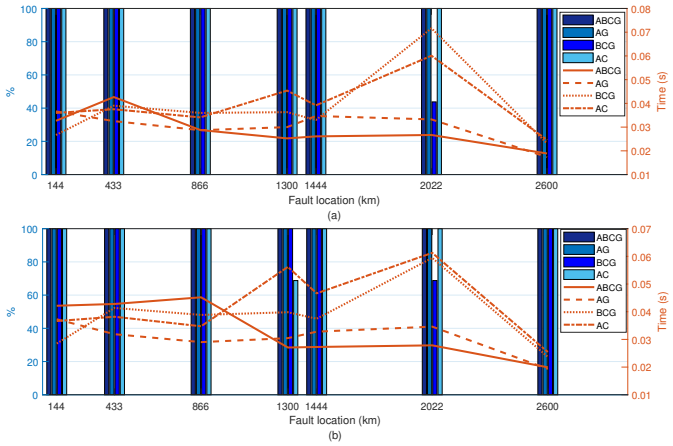

Fig. 9. Average fault detection time and success rate for fault resistance of 0.01 Ω (a) and 10 Ω (b) - All types of faults.

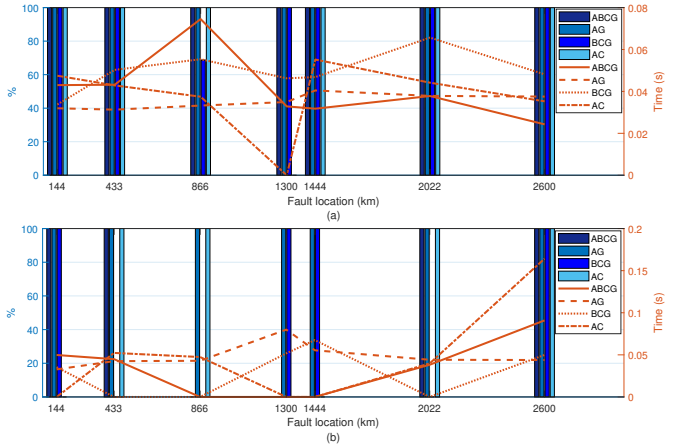

Fig. 10. Average fault detection time and success rate for fault resistance of 50 Ω (a) and 100 Ω (b) - All types of faults.

Fig. 9 shows the results for R_f of 0.01 Ω and 10 Ω. It can be observed that the algorithm is robust and sensitive, ensuring 100% of success throughout the entire line for R_f=0.01 Ω (Fig. 9a), except for BCG faults. The time response is small for most types of faults, even for faults at the middle of the line, ranging from [17:70] ms. Faults with $R_f = 10$ Ω (Fig. 9b) are fully identified, but the AC fault at 1300 km has a success rate that decreases to 68%. BCG faults have an increase in the success rate, reaching 68%. The average time detection ranges as [19:61] ms, and ABCG fault detection was the fastest in the central region. ABCG faults near the terminals were properly identified with the three reference points.

Fig. 10 shows the results for all types of faults with R_f of 50 Ω and 100 Ω. As observed previously, the algorithm loses sensitivity for some fault types as the fault impedance increases. Fig. 10 shows that the LL fault was not identified in the middle of the line (AC fault). For other fault locations, the algorithm succeeded with an average time response near 60 ms. The ABCG was identified throughout the line, but the time response for the fault at one location was slow (75 ms). If we consider the circuit-breaker response time (50 ms), the HWL would be tripped after 100 ms. The AG fault time response ranges in [35:40] ms.

We can expect that when the fault resistance increases, the algorithm will fail for faults not involving ground in more locations, as shown in Fig. 10b for R_f=100 Ω. The AG fault was always identified along the entire line length with adequate time response, ranging in [32:79] ms. The ABCG fault was only identified near the terminals, and the time response ranges in [45:91] ms. The algorithm fails for the phase-to-phase faults (AC and BCG) in some fault locations. When the protection manages to identify, the response time can be below 60 ms, but at the remote terminal, the algorithm took 100 ms to send the binary signal up. This result can be enhanced if fault classification loops are included in the algorithm.

In the central region of the HWL line, fault detection had a slower response and was less accurate. Many factors can cause high time detection and lower accuracy, particularly for phase-to-phase-to-ground faults. The imposed time delay of terminals' data and the restriction threshold established have a major impact on these results. There is not much to be done to

improve the communication channel latency, but the restriction threshold can be better adjusted if fault classification loops are considered, which is planned for future research.

V. Conclusions

This study developed an innovative protection scheme for a half-wavelength transmission line called the power differential protection algorithm. Protection was demonstrated to be robust and reliable in a software-in-the-loop time-domain environment. The long HWL line has a unique fault response that needs a specific protection design, similar to long HVDC links. Existing protection systems cannot detect faults through an HWL line, primarily with faults in the central region, which has a natural high impedance characteristic.

Due to its peculiarities, an HWL transmission line must have an overvoltage mitigation method, specifically SGs that are located at the centre of critical resonant regions. The SGs operate for three-phase, phase-to-phase-to-ground, and phase-to-phase faults in the resonant region and do not compromise the proposed algorithm response.

To manage the long line length, three reference points for capacitive current compensation were used to enhance the algorithm response, resulting in the entire line protection for all types of faults for fault resistance up to 10 Ω. The algorithm has low sensitivity to high fault impedance: the response was successful but slower for phase-to-ground faults and had no action for phase-to-phase-to-ground, phase-to-phase and three-phase faults. This low sensitivity is caused by the selected thresholds. However, the established values are necessary to distinguish internal from external faults. For $0.01\ \Omega$, the algorithm had 100% success and was faster. For $100\ \Omega$, the algorithm failed near the middle of the line for ABCG, BCG and AC faults.

Regarding the algorithm time response, protection was compromised by the imposed time delay between the terminals. However, this characteristic is expected with long transmission systems and exists in HVDC systems. The detection time can be considered satisfactory because it achieves the typical protection system requirements. Although the algorithm is not as fast as the typical protections used in conventional long lines, it provides high reliability, which is essential in a bulk power transmission system.

References

[1] F. S. Prabhakara, K. Parthasarathy and H. N. R. Rao, *Analysis of Natural Half-Wave-Length Power Transmission Lines*, IEEE Transactions on Power Apparatus and Systems, PAS-88, n. 12, p. 1787–1794, 1969.

[2] F. Iliceto, and F. M. Gatta, *Analysis of Half-Wave Length Transmission Lines with Simulation of Corona Losses*. IEEE Transactions on Power Delivery, vol. 3, pp. 2081-2089, 1988.

[3] F. J. Hubert and M. R. Gent, *Half-Wavelength Power Transmission Lines*, IEEE Spectr., vol. 2, no. 1, pp. 87–92, Jan. 1965.

[4] D. F. Jimenez and O. Dias and M. C. Tavares, *Fault classification and phase selector algorithm for half-wavelength transmission lines.* Electric Power Systems Research, 203, 1-10, 107637, 2022.

[5] J. S. Ortega and M. C. Tavares, *Transient Analysis and Mitigation of Resonant Faults on Half-Wavelength Transmission Lines*, IEEE Transactions on Power Delivery, vol. 35, no. 2, pp. 1028, 2020.

[6] J. S. Ortega and M. C. Tavares, *Analysis of Half-Wavelength Transmission Line Under Critical Balanced Faults: Voltage Response and Overvoltage Mitigation Procedure*, Electric Power Systems Research, vol. 166, pp. 99–111, 2019.

[7] B. F. Küsel, F. V. Lopes and K. M. Silva *Unconventional Distance Protection in Half-Wavelenght Transmission Lines*, International Conference on Power Systems Transients (IPST), Cavtat, Croatia, 2015.

[8] X. Ma, M. Zhang, J. Gao, Q. Wang, Z. Bo, Y. Zhao and Y. I. Zhu, *Adaptability Analysis of Differential Protection for UHV Half-wavelength AC Transmission Line*, China International Conference on Electricity Distribution,pp. 1-6, 2016.

[9] P. Shao, Y. Li, R. Fang, X. Guo. *An improved Bergeron differential protection for half-wavelength AC transmission line*, E3S Web of Conferences, 257, 01016, 2021.

[10] N. Tong, L. Chen, W. Wang, X. Lin, Z. Li. *Local-Measurement-Based High-Speed Protection for Half-Wavelength UHV Lines*. IEEE Transactions on Power Delivery, 35(5), 2481–2494, 2020.

[11] G. Yarong, Z. Zexin, W. Xingguo and L. Huanzhang, *Time Difference Method to Calculate the Optimal Differential Point of Half-wavelength AC Transmission Line Differential Protection*, IEEE Innovative Smart Grid Technologies - Asia (ISGT Asia), pp. 1193-1198, 2019.

[12] S. Deotale and A. A. Dongre, *Performance Analysis of Power Differential Based Transmission Line Protection*, International Conference on Energy, Communication, Data Analytics and Soft Computing, pp. 342-345, 2017.

[13] H. Wu, X. Dong and Q. Wang, *A New Principle for Initial Traveling Wave Active Power Differential Busbar Protection*, IEEE Access, vol. 7, pp.70495-70512, 2019.

[14] A. F. N. C. Moro and J. S. Ortega and M. C. Tavares.*Performance evaluation of power differential protection applied to half-wavelength transmission lines*, Electric Power Systems Research, 209, 107998, 2022.

[15] M. L .S. Almeida and K. M. Silva. *Transmission Lines Differential Protection Based on an Alternative Incremental Complex Power Alpha Plane*. IET Generation, Transmission and Distribution, 11(1), pp.10–17, 2017.

[16] E. O. Schweitzer and D. Hou. *Filtering for Protective Relays*, IEEE WESCANEX 93 Communications, Computers and Power in the Modern Environment - Conference Proceedings, pp. 15-23, 1993.

[17] A. G. Phadke and J. S. Thorp. *"Synchronized phasor measurements and their applications"*, Springer,Power Electronics and Power Systems, 2010.

[18] Z. Y. Xu and Z. Q. Du and L. Ran and Y. K. Wu and Q. X. Yang and J. L. He, *A Current Differential Relay for a 1000-kV UHV Transmission Line*, IEEE Transactions on Power Delivery, vol. 22, no. 3, pp. 1392-1399, 2007.

[19] K. M. Silva and M. L. S. Almeida, *Positive Sequence Voltage Memory Filter for Numerical Digital Relaying Applications*, Electronics Letters ,vol 51, pp. 1697-1699, October, 2015.